

## Biocomposite hydrogel beads from glutaraldehyde-crosslinked phytochemicals in alginate for effective removal of methylene blue



Andreas Andreas <sup>a,1</sup>, Zefanya Gerald Winata <sup>a,1</sup>, Shella Permatasari Santoso <sup>a,b,\*</sup>, Artik Elisa Angkawijaya <sup>c</sup>, Maria Yuliana <sup>a</sup>, Felycia Edi Soetaredjo <sup>a,b</sup>, Suryadi Ismadji <sup>a,b</sup>, Hsien-Yi Hsu <sup>d,e</sup>, Alchris Woo Go <sup>c</sup>, Yi-Hsu Ju <sup>b,c,f</sup>

<sup>a</sup> Chemical Engineering Department, Faculty of Engineering, Widya Mandala Surabaya Catholic University, Surabaya 60114, East Java, Indonesia

<sup>b</sup> Chemical Engineering Department, National Taiwan University of Science and Technology, Taipei 10607, Taipei, Taiwan

<sup>c</sup> Graduate Institute of Applied Science and Technology, National Taiwan University of Science and Technology, Taipei 10607, Taipei, Taiwan

<sup>d</sup> School of Energy and Environment & Department of Materials Science and Engineering, City University of Hong Kong, 83 Tat Chee Ave, Kowloon Tong, Hong Kong, China

<sup>e</sup> Shenzhen Research Institute of City University of Hong Kong, Shenzhen 518057, China

<sup>f</sup> Taiwan Building Technology Center, National Taiwan University of Science and Technology, #43 Keelung Rd., Sec. 4, Daan Dist., Taipei 10607, Taiwan

### ARTICLE INFO

#### Article history:

Received 5 October 2020

Received in revised form 30 January 2021

Accepted 3 February 2021

Available online 05 February 2021

#### Keywords:

Alginate bead

Red cabbage extract

Phytochemicals

Adsorption methylene blue

Intraparticle diffusion

### ABSTRACT

Phytochemicals, i.e., flavonoids, phenolics, and anthocyanin, extracted from red cabbage, were crosslinked with alginate to prepare biocomposite hydrogel beads (BHB). The preparation of BHB involved three consecutive steps: (1) extraction and solvent reduction of phytochemicals from red cabbage, (2) crosslinking of phytochemicals into alginate matrix using glutaraldehyde, and (3) formation of the hydrogel beads in  $\text{CaCl}_2$  solution. The resulting BHB sorbents were characterized using scanning electron microscopy (SEM), Fourier transform infrared spectroscopy (FTIR), and X-ray diffraction (XRD) analyses. The cross-section structure of the BHB was confirmed from the SEM images. The alteration of FTIR peaks implied the success of the crosslinking of phytochemical compounds into the alginate. The adsorption equilibrium and kinetic studies of BHB were conducted using basic blue 9 (BB9) as the model adsorbate. FTIR characterization of the BHB post-adsorption reveals the functional groups of the adsorbent involved in the dye adsorption. The calculated adsorption isotherm, kinetics, and thermodynamic parameters show good agreement with the characterization results of adsorbate post-adsorption. The adsorption isotherm is being in congruence with the Langmuir model, and the highest adsorption capacity recorded was  $1442.0 \text{ mg g}^{-1}$  at 323 K and pH of 11.0. Adsorption kinetics was better fitted to the pseudo 1st order model than the pseudo 2nd order and Elovich models, which further support the dye physisorption behavior. The initial adsorption rate was influenced by the rapid surface adsorption followed by intraparticle diffusion. The thermodynamic parameters show the spontaneity of the adsorption, and the adsorption proceeds endothermically. The cost analysis shows the economic feasibility of BHB sorbent production for adsorption applications.

© 2021 Elsevier B.V. All rights reserved.

## 1. Introduction

The growth of the textile industry can be beneficial to satisfy the clothing demands of the globally ever-growing population. However, the rapid growth of the textile industry can bring a negative impact to the environment as one of the water contamination sources. The substantial amount of water used in the textile-dyeing process often results in difficulties in managing the wastewater, where over  $200 \text{ m}^3$  of water is used for the textile dyeing process per day [1]. The discharged wastewater from the dye production, which is rich in dyes and heavy metals, is often directly disposed into the water bodies [2]. Globally, there are

more than 700,000 tons of dyes are produced annually. And, with the current expected Compound Annual Growth Rate of 5.9% and at least 2% of dyes were discharged in the aqueous eluent, it is expected that at least 120,000 tons of dyes leaked to water bodies [3–5]. Among the wide variety of dyes, cationic dyes (e.g., methylene blue) are well known to be the most problematic due to their photo-reactivity, which is destructive to the aquatic biota. Light exposure to methylene blue produces single oxygen, which can cause cell damage and consequent cell death [2,6,7].

Various water and wastewater treatment techniques have been developed in the past few decades and are widely applied in industrial-scale applications, including filtration, membrane dialysis, coagulation/flocculation, ion exchange, precipitation, electrochemical treatment, and adsorption. The combination of these techniques has also been frequently used to treat complex wastewater, where adsorption is often employed as the first step before any other techniques. In this regard,

\* Corresponding author at: Chemical Engineering Department, Faculty of Engineering, Widya Mandala Surabaya Catholic University, Surabaya 60114, East Java, Indonesia.

E-mail address: [shella\\_p5@yahoo.com](mailto:shella_p5@yahoo.com) (S.P. Santoso).

<sup>1</sup> These authors contribute equally.

the adsorption process offers a number of advantages, including simplicity and flexibility in the design and operation, cleaner and harmless effluents post-usage, as well as safe and economical. With respect to dye-contaminated water, adsorption techniques have been widely applied, mainly due to the ease of adjusting the adsorbent binding sites so that dye removal in low concentrations is possible [8–12].

The utilization of sodium alginate (Alg) as a versatile biopolymer has been extensively described in many advanced applications, such as 3D printing, wound dressing, adsorption, and food packaging. In the adsorption technology, a variety of Alg (in its Alg-hydrogel form) was used as an adsorbent for a range of adsorbate-from drug to hazardous materials such as heavy metals, organic compounds, and dyes. In addition, various modification strategies of Alg-based hydrogels (HAlg) have been reported in an effort to enhance the adsorption capacity. For example, the modifications using clay minerals (e.g., zeolite and bentonite) can promote the adsorption capacity of HAlg [13–15]. This promotion is predictable because the clay minerals are known as super-adsorbents. However, the increase in adsorption results was not as high as expected because the layer of Alg particles blocked most of the surface area of the clay minerals. Nonetheless, the HAlg/clay mineral composite adsorbents have advantages in terms of environmental friendliness, low-cost, and ease of preparation. Fabrication of HAlg using natural bioactive compounds containing oxygen functional groups is another facile method that can promote adsorption ability. In 2012, a study reported the modification of Alg-based hydrogels using humic acid, which may improve its adsorption capacity [16]. The incorporation of oxygen-containing functional groups, such as hydroxyl, carboxylates, and amine groups, to the HAlg surface is postulated to enhance the adsorption capacity by providing active sites for adsorbate binding. These functional groups can increase adsorption capacity by contributing to the electrostatic interactions, especially toward charged solutes (e.g., cationic dyes, anionic dyes, and metal ions).

In this study, we attempted to combine the crude plant extract containing bioactive compounds (i.e., phenolic, flavonoids, and alkaloids) with Alg-based hydrogel beads for improved adsorption capacity. Red cabbage extract was used as the model since it has been well-known for its high polyphenols content (i.e., anthocyanins, phenolics, and flavonoids). These polyphenols are known to possess various functional groups, such as hydroxyl (OH), methoxide ( $\text{OCH}_3$ ), and carboxyl ( $\text{COOH}$ ) [17]. Incorporating these functional groups onto the Alg matrix can provide additional adsorption sites that lead to the adsorption capacity enhancement. To the best of our knowledge, our group is the first to report an increase in the adsorption capacity of Alg-based adsorbents after being modified with plant crude extract. A single adsorption system was studied on the pristine and modified Alg-based hydrogel beads against methylene blue dye (also known as Basic Blue 9, BB9) to investigate the effect of plant crude extract modification. The effects of several operating parameters (i.e., temperature, solution pH, and contact time) on the adsorption performance of Alg-based composite hydrogel beads were investigated and thoroughly discussed.

## 2. Materials and methods

### 2.1. Materials

Red cabbages were purchased from a local traditional market in Surabaya, East Java, Indonesia. Sodium alginate (5.0–40.0 cps in viscosity) was obtained from a local chemical distributor (C.V. Nura Jaya). Technical grade ethanol (96% purity) was purchased from Indofa Utama Multi Core company (Indonesia). Calcium chloride ( $\text{CaCl}_2$ , 98.0% purity), glutaraldehyde (GA, 25 wt% solution), basic blue 9 (BB9, CI 52015) were obtained from Merck Millipore (Germany). Acetic acid glacial (99.5% purity) was supplied by Sigma-Aldrich (USA).

### 2.2. Preparation of red cabbage extract (RCE)

3.0 kg of fresh red cabbages (RC) were cut into small pieces and crushed using a blender to obtain RC juice. A 5.0 L of the solvent mixture consisting of 1:1 (v/v) ethanol/water was prepared, followed by acidification to a pH ~3 with acetic acid glacial. The as-prepared solvent was then added to the RC juice, and the mixture was shaken in a shaker bath. The process was conducted in a closed container at room temperature overnight. Subsequently, the RC cake was filtered and the RC extract (RCE) was collected. The RCE solution was then centrifuged at 5000 rpm to remove the remaining cake residue. Afterward, the RCE solution was slowly concentrated by evaporating the solvent at 40 °C using a rotary evaporator until about 1.0 L of viscous solution was obtained. The total flavonoid content (TFC), total phenolic content (TPC), and total anthocyanin content (TAnC) of the RCE was determined according to the previously reported method [18] and the results are found to be: KFC = 590.06 ± 0.81 mg quercetin/L, TPC = 697.52 ± 4.67 mg gallic acid/L, and TAnC = 250.35 ± 2.70 mg L<sup>-1</sup>.

### 2.3. Preparation of biocomposite hydrogel beads (BHB)

To prepare BHB, 3 wt% of Alg powder was added slowly into 100 mL of RCE. The solution was stirred in a closed glass container for 1 h to obtain a homogenous viscous solution. The viscous solution was then dripped into a 3 wt% aqueous  $\text{CaCl}_2$  solution using a 1000  $\mu\text{L}$  micropipette to obtain the hydrogel beads. The obtained beads had an average diameter of 4.5 mm. Subsequently, the resulting beads were immersed into a 1 wt% glutaraldehyde (GA) overnight to crosslink the Alg and the phytochemicals in RCE. The beads were then collected and thoroughly rinsed with distilled water. The beads were kept in a plastic-vacuum bag and stored in the refrigerator before use. In this work, beads were used directly or stored for a maximum of 1 day before use.

### 2.4. Characterization of the BHB adsorbents

The surface functional groups were determined using Fourier transform infrared spectroscopy (FTIR) using a Shimadzu/FTIR-8400S spectrophotometer. The surface morphology was examined by scanning electron microscopy (SEM) analysis on a field-emission JEOL JSM-6390. The point-of-zero-charge (PZC), which is defined by the point where the curve  $\text{pH}_{\text{final}}$  vs.  $\text{pH}_{\text{initial}}$  crosses the line  $\text{pH}_{\text{final}} = \text{pH}_{\text{initial}}$ , was determined according to the previously reported procedure [19].

### 2.5. Adsorption study

#### 2.5.1. Preliminary experiments

In this work, the BHB sorbent was prepared from the combination of Alg, GA, and RCE (Alg/GA/RCE). A preliminary experiment was conducted to assess the adsorption performance of the Alg/GA/RCE with the unmodified Alg and the Alg/RCE beads (without GA crosslinking). Briefly, the unmodified Alg beads were prepared by dissolving 3 wt% of Alg powder in 100 mL distilled water. Meanwhile, the Alg/RCE was prepared by dissolving 3 wt% of Alg powder in 100 mL RCE. The resulting Alg and Alg/RCE hydrogel beads were then obtained by dropping the respective solutions into a 3 wt% of  $\text{CaCl}_2$  solution. The obtained hydrogel beads were then collected and rinsed with distilled water.

The adsorption capacity of the three hydrogel bead samples, namely Alg, Alg/RCE, and Alg/GA/RCE was compared. One bead (1.47 ± 0.07 g wet weight and 0.03 ± 0.00 g dry weight) of each sample was added to BB9 solutions at three different concentrations (i.e., 100, 300, and 500 ppm). The adsorption tests were then allowed to run for 8 h at 30 °C to reach an equilibrium. The residual concentrations of BB9 were measured using a spectrophotometric technique in a Shimadzu UV/Vis spectrophotometer at  $\lambda_{\text{max}}$  of 663 nm.

### 2.5.2. Adsorption study

The effect of pH on the adsorption of BB9 dye on Alg/GA/RCE BHB was evaluated over a pH range from 2 to 12 with an initial dye concentration of 100 mg L<sup>-1</sup> and a constant adsorbent mass of 0.03 g. The pH was adjusted using 0.1 N HCl or NaOH solutions and detected using the Mettler Toledo digital pH meter. The adsorption process was carried out for 8 h at room temperature using a Memmert shaking water bath. The percentage of dye removal (%R) by the adsorbent at each pH condition was calculated according to Eq. (1):

$$\%R = \frac{(C_0 - C_e)}{C_0} \times 100\% \quad (1)$$

where  $C_0$  and  $C_e$  are the concentration of BB9 at initial and equilibrium (mg L<sup>-1</sup>), respectively.

Adsorption isotherm experiments were conducted using 25 mL of BB9 solution with various initial concentrations of 100–2000 mg L<sup>-1</sup>. A known amount of adsorbent was introduced into a series of conical flasks containing BB9 solution. Subsequently, the flasks were placed in a Memmert shaking water bath for 8 h at a specific temperature (i.e., 303, 313, and 323 K). The adsorbent was then separated from the BB9 solution by filtration. The equilibrium concentration of BB9 solution after adsorption was quantitatively determined using a Shimadzu UV/Vis spectrophotometer at a  $\lambda_{max}$  of 663 nm. The equilibrium adsorption capacity ( $Q_e$ , mg g<sup>-1</sup>) was calculated using the following equation:

$$Q_e = \frac{(C_0 - C_e) \times V}{m} \quad (2)$$

where  $m$  is the mass of adsorbent added into BB9 solution (g) and  $V$  is the volume of the BB9 solution in (L).

The adsorption kinetic experiments were investigated at three different initial concentrations of BB9 (i.e., 300, 500, 700, and 1000 mg L<sup>-1</sup>). The amount of BB9 adsorbed was measured at an hour interval until a certain plateau (or no further changes in concentration) was achieved. The amount of BB9 dye adsorbed at a given time ( $Q_t$ , mg g<sup>-1</sup>) was calculated according to Eq. (2), with the symbol “e” corresponding to the equilibrium state is replaced by “t”, which refers to the state at a given time.

## 3. Results and discussion

### 3.1. Characterization of the BHB adsorbents

SEM, FTIR spectroscopy, and XRD characterizations were performed to examine the characteristics of BHB prepared from Alg/GA/RCE and compare to those of unmodified-Alg and Alg/RCE samples. The FTIR spectra showing the functional groups of the adsorbent materials are presented in Fig. 1a. The presence of new absorption bands corresponding to the polyphenol compounds of RCE was indicated by asterisks (\*), for example the absorption peak at 1512 cm<sup>-1</sup> for Alg/RCE and Alg/GA/RCE samples corresponds to the C=O stretching vibration of the methoxy (OCH<sub>3</sub>) groups. Other peaks corresponding to the polyphenol compounds present in the Alg/RCE and Alg/GA/RCE samples are located at 644 and 677 cm<sup>-1</sup>, respectively, which can be assigned to the out-of-plane bending vibration of methyl groups. Furthermore, the presence of GA crosslinking in the Alg/GA/RCE was confirmed by the absorption band at 1697 cm<sup>-1</sup>, which corresponds to the C=O stretching vibration of the aldehyde group.

Other characteristic absorption bands of Alg/RCE and Alg/GA/RCE samples are similar to that of Alg, which is reasonable since Alg itself contains identical functional groups with the polyphenols (e.g., -OH and -COOH). The observable characteristic bands are as follows: the free -OH vibration band was indicated by the presence of a broad-spectrum at a wavenumber range of 3600–3200 cm<sup>-1</sup>. The absorption band detected at 2901 cm<sup>-1</sup> in unmodified-Alg indicates the aliphatic C-H stretching [20], the disappearance of this peak in Alg/RCE and Alg/GA/RCE samples is due to the crosslinking of GA to the Alg polymer chain.

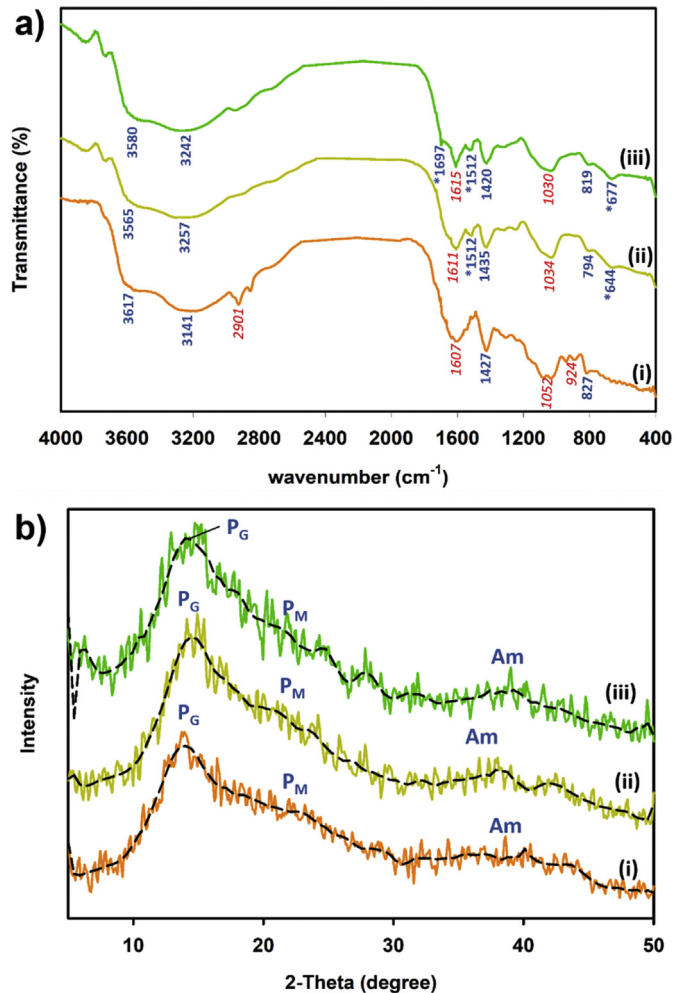


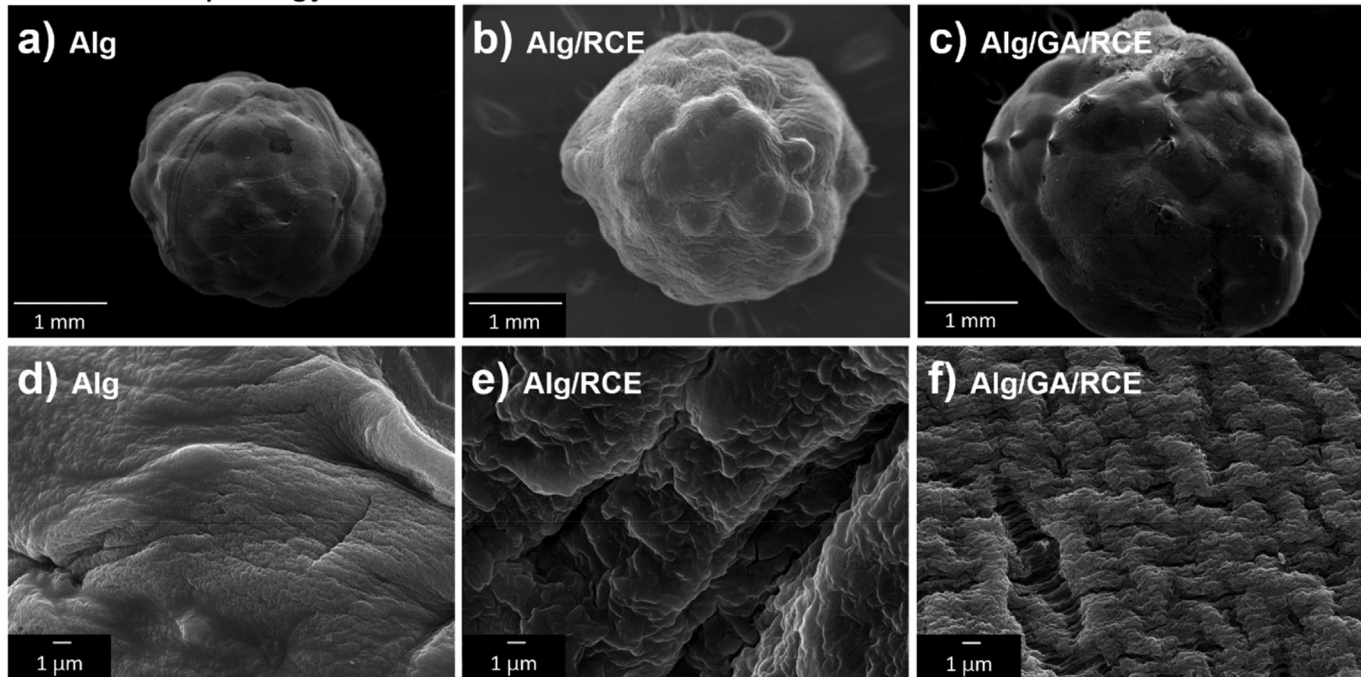
**Fig. 1.** (a) FTIR spectra and (b) XRD patterns showing polyguluronate (P<sub>G</sub>), polymannuronate (P<sub>M</sub>), and amorphous halo (Am) units for (i) Alg, (ii) Alg/RCE, and (iii) Alg/GA/RCE BHB samples.

GA/RCE sample can be attributed to the coordination of this group with the polyphenols of RCE. The stretching vibration of the C=O group was detected at 1607 cm<sup>-1</sup> for unmodified-Alg, 1611 cm<sup>-1</sup> for Alg/RCE, and 1615 cm<sup>-1</sup> for Alg/GA/RCE. The anti-symmetric -COO<sup>-</sup> vibration band was observed for all samples at ~1430 cm<sup>-1</sup>. The peak observed at ~1030 cm<sup>-1</sup> for all samples corresponded to the partial-covalent bonding of Ca and oxygen atom to form the hydrogel beads [20,21]. The presence of guluronate and mannuronate units (the specific units of Alg polymer chain) was indicated by a band at ~810 cm<sup>-1</sup> [20,21].

The XRD patterns (Fig. 1b) of the as-prepared hydrogel beads all show the characteristic Bragg reflections associated with the primary units of Alg polymer, namely polyguluronate (P<sub>G</sub>), polymannuronate (P<sub>M</sub>), and amorphous halo (Am) units [22]. The peak of the P<sub>G</sub> unit was observed at 20 of 13.9°, 14.6°, and 14.1° for unmodified-Alg, Alg/RCE, and Alg/GA/RCE samples, respectively. The P<sub>M</sub> unit was observed at 20 of 22.9°, 21.4°, and 21.8°. And, the Am unit at 2-Theta 38.6, 37.4, and 39.0°. It appears that the crosslinking of RCE to Alg only causes an unnoticeable shifting of the XRD peaks and does not cause the alteration of the XRD pattern.

The SEM images of the surface and cross-section morphologies of the three BHB particles (i.e., Alg, Alg/RCE, and Alg/GA/RCE) are displayed in Fig. 2. As can be seen in Fig. 2a–c, all three BHB samples exhibit a globular shape. Higher magnification images (Fig. 2d–f) reveal that the Alg beads have a smoother surface than those of Alg/RCE and

## Surface morphology



## Cross-section morphology

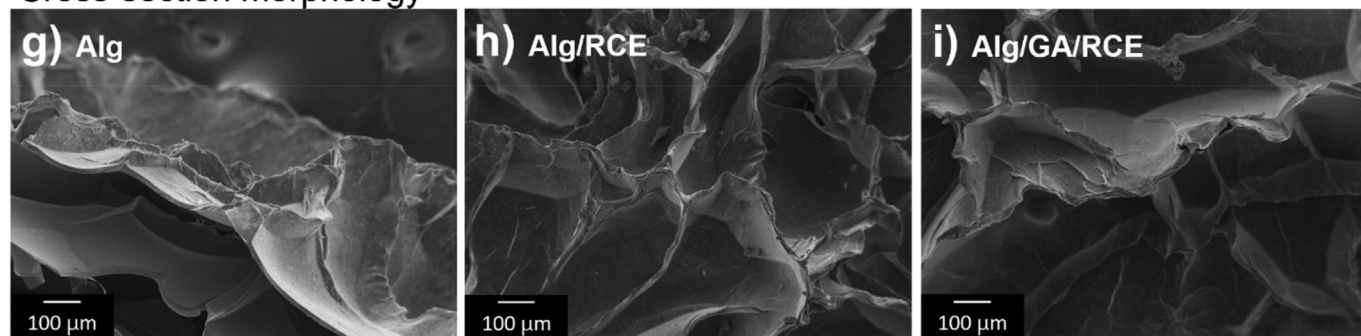


**Fig. 2.** (a-c) SEM images the whole spherical shape of Alg, Alg/RCE, and Alg/GA/RCE BHB. (d-f) SEM images showing the surface morphology Alg, Alg/RCE, and Alg/GA/RCE BHB. (g-i) SEM images showing the cross-section of Alg, Alg/RCE, and Alg/GA/RCE BHB.

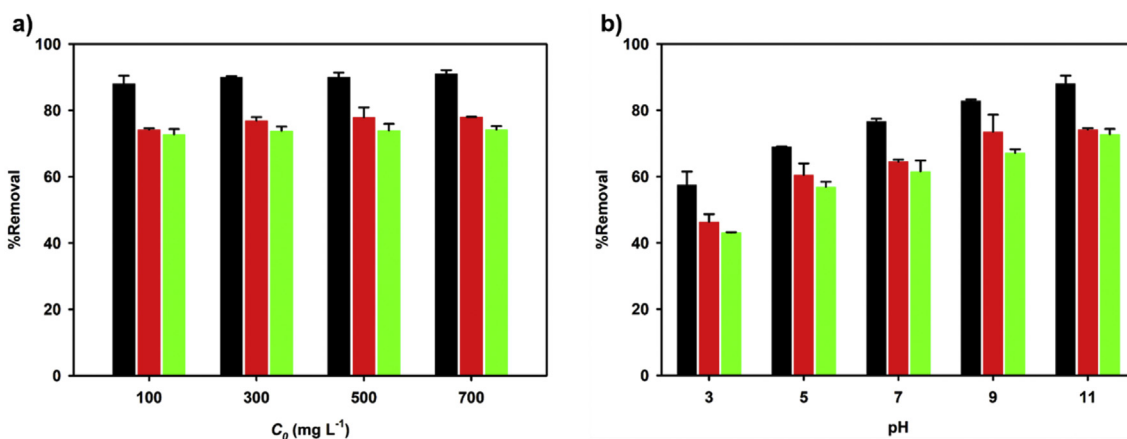


**Fig. 3.** (a) %Removal of BB9 at a different initial concentration ( $C_0$ ) using different Alg-based adsorbent, adsorption was conducted using 0.03 g of the adsorbent for 8 h at 30 °C, and pH of 11. (b) %Removal of BB9 at different pH, adsorption was conducted using 0.03 g of the adsorbent for 8 h at 30 °C, and  $C_0$  of 100  $\text{mg L}^{-1}$ . The green bar, red bar, and black bar show the properties of Alg, Alg/RCE, and Alg/GA/RCE, respectively.

Alg/GA/RCE samples, implying that the incorporation of polyphenols into Alg induces a change in the gelation properties. The change in the gelation properties of Alg can be attributed to the interaction of polyphenols with the Alg matrix [23,24]. In the Alg/GA/RCE sample, some cavities on the particle surface resembling large macropores are evident (Fig. 2f). The formation of such surface cavities can be ascribed to the presence of polyphenols in the Alg matrix that provides additional functional groups (i.e., OH, OCH<sub>3</sub>, and COOH), which may limit the diffusion of Ca<sup>2+</sup> into the Alg matrix [24,25], and thus reduce the gelling ability. The cross-sectional morphology of all three BHB particles is shown in Fig. 2g–i, characterizing the nonporous structure with a crater-like topography and relatively smooth surface.

### 3.1.1. Effect of pH and initial adsorbate concentration on the adsorption of BB9 dye

The solution pH and the initial adsorbate concentration play important roles in determining the adsorption performance of an adsorbent [26–28]. Fig. 3a shows the effect of the initial adsorbate concentrations on the percentage of dye removal by three BHB sorbents. It can be seen that the Alg/GA/RCE exhibits the highest removal efficiency of BB9 at all initial dye concentrations ( $C_0$ ). The removal capacity of the Alg/RCE is also slightly higher than that of pristine Alg. These results suggest that the incorporation of RCE-derived polyphenols provides additional adsorption sites to accommodate higher amounts of dye molecules. More importantly, the presence of GA cross-links can aid in strengthening the binding of polyphenol molecules within the hydrogel bead. Without the GA cross-links, these polyphenols are weakly bound to the Alg surface and can be removed easily during the preparation, thus leading to only a marginal increase in the removal efficiency of Alg/RCE compared to that of Alg. Thus, the enhanced adsorption capacity of Alg/GA/RCE can be mainly attributed to the cross-linking of RCE by GA, which allows for an increased amount of polyphenols to be strongly bound within the Alg matrix. Furthermore, the higher removal efficiency of Alg/GA/RCE can be attributed to the presence of cavities on the surface of the sorbent (as evidenced by the SEM image in Fig. 2f), which may increase the pore volume of the materials and result in superior removal efficiency.

Fig. 3b shows the effect of solution pH on the removal performance of BHB samples toward BB9. In this regard, the alkaline pH conditions cause the deprotonation of surface functional groups of the BHB adsorbents, such as hydroxyl (OH) and carboxyl (COOH) groups, thus providing a net negative charge on the surface. Experimental support for this statement is provided by the PZC measurement shown in Fig. 4a. The PZC value of the Alg/GA/RCE BHB was found to be 7.7, which implies that the adsorbent bears a negative surface charge at pH conditions higher than the pH<sub>PZC</sub>. Meanwhile, the BB9 molecules are present in the cationic form at high pH [29]. Accordingly, the different charges between these two species lead to the attractive interaction of BB9 dye cations onto the negatively charged surface of BHB. The magnitude of the negative charge also becomes greater at higher alkaline pH and therefore the removal efficiency of BB9 was higher at pH 11 than that at pH 9. A similar phenomenon was also observed in other studies, in which the adsorption of Alg-based materials becomes more pronounced at higher pH values [14,30]. Note that the small difference in removal efficiency between Alg (72.8%) and Alg/RCE (74.2%) at pH 11 could be mainly ascribed to the partial loss of available adsorption sites of the latter due to the enhanced degradation of some polyphenols under such highly alkaline condition [31,32]. Better BB9 removal at alkaline pH could also be related to the swelling ability of BHB sorbent. Immense particle swelling occurs at a more alkaline pH, which is due to the chain expansion induced by the presence of deprotonated carboxyl groups on the Alg backbone [33]. More significant particle swelling at pH 11 (Fig. 4b) could afford more contact areas on the surface of BHB, thus allowing an enhanced electrostatic interaction with cationic BB9 molecules.

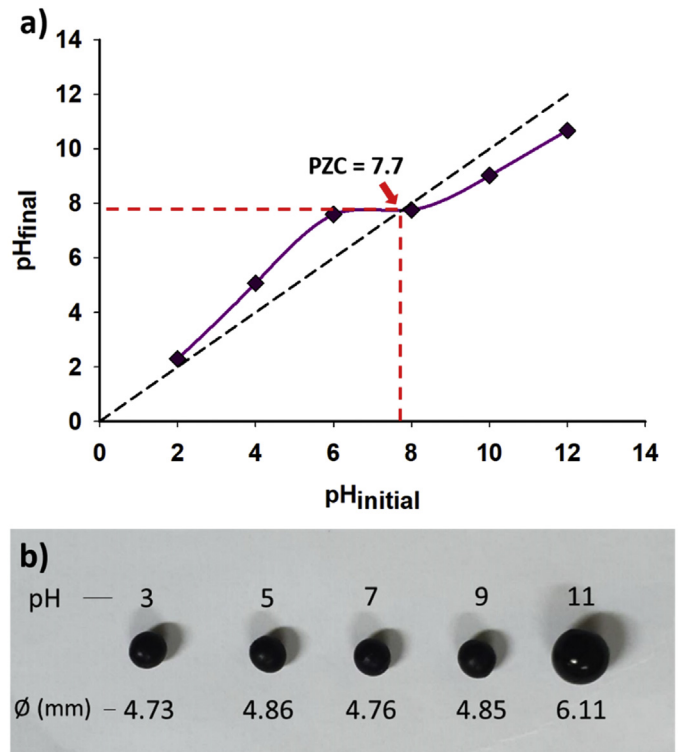


**Fig. 4.** (a) The point-of-zero-charge (PZC) value of Alg/GA/RCE BHB. (b) Swelling diameter ( $\emptyset$ ) of the Alg/GA/RCE BHB after adsorption of BB9 at different pH conditions.

### 3.2. Adsorption mechanism of BB9 onto BHB

The FTIR spectra of pristine and BB9 loaded-BHB adsorbents are recorded to elucidate the dye adsorption mechanism. As shown in Fig. 5a, several distinct spectral features were observed after dye sorption, as highlighted by the four blue regions. In the highlighted area (i), the shape and intensity of the peak corresponding to the free OH group are altered significantly. This suggests that the surface hydroxyl group plays an active role in the adsorption of BB9. In region (ii), the band at 1615 cm<sup>-1</sup> corresponding to the carboxyl group was altered in shape and shifted to 1623 cm<sup>-1</sup>, which suggests an interaction between BB9 and the C=O group of the adsorbent. The vibration band of the group at 1030 cm<sup>-1</sup>, at the area (iii), was still observed in the spectra before and after dye adsorption. However, the band shape was differing significantly; this can be due to the inclusion of BB9 molecules in the internal structure of the crosslinked group of the adsorbent. In the blue area (iv), new peaks are observed in the spectral of adsorbent post-adsorption. The peaks could be attributed to the C-Cl vibration bands originating from the Cl<sup>-</sup> ions of BB9. The Cl<sup>-</sup> ions may also be adsorbed from the bulk solution during the adsorption process.

The XRD pattern of the BHB post-adsorption is presented in Fig. 5b. It can be shown that there is no apparent change observed in the XRD patterns of the adsorbent before and after dye adsorption. This result suggests that no structural alteration of the adsorbent and physisorption plays a dominant role in the dye uptake.

### 3.3. Adsorption isotherm

An adsorption isotherm study of BB9 on three BHB samples was conducted to gain insight into the adsorption behavior. The classical two-parameter models, namely Langmuir and Freundlich, were applied to correlate equilibrium adsorption data and predict the homogeneity of adsorbate distribution on the adsorbent surface area. The Langmuir isotherm model was developed based on the assumption of monolayer

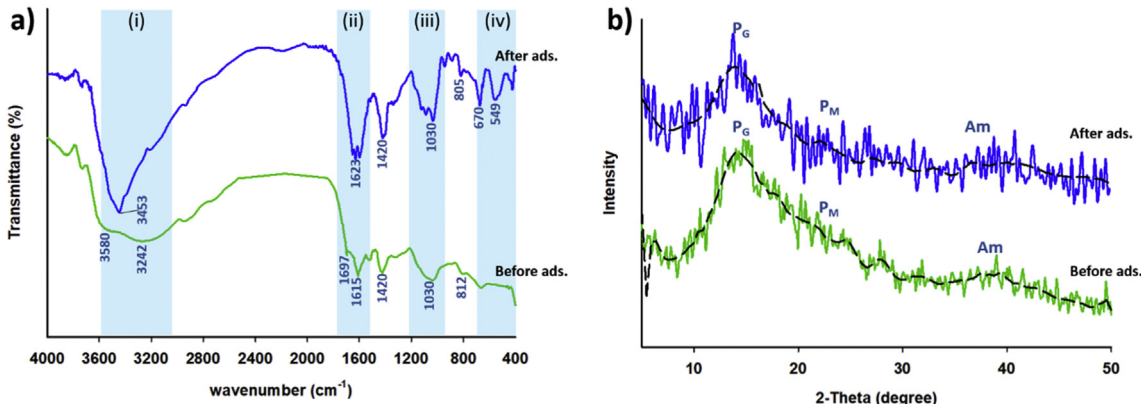


**Fig. 5.** (a) FTIR spectra and (b) XRD patterns of BHB before and after the adsorption process of BB9. The blue-highlighted areas in FTIR spectra show the apparent alteration in the spectral features of BHB post-adsorption of BB9 dye.

formation of adsorbate molecules on a homogeneous surface [34]. The nonlinear mathematical model of Langmuir is expressed as follows:

$$Q_e = \frac{Q_{L,\max} K_L C_e}{1 + K_L C_e} \quad (3)$$

where  $Q_{L,\max}$  is the theoretical maximum adsorption capacity (mg g<sup>-1</sup>),  $K_L$  is a fit parameter related to the affinity between the adsorbent and the adsorbate (L mg<sup>-1</sup>), and  $Q_e$  represents the equilibrium adsorption capacity (mg g<sup>-1</sup>). Meanwhile, the Freundlich model was established based on the multilayer adsorption assumption over the heterogeneous solid surface [35]. The mathematical expression of Freundlich is given in Eq. (4):

$$Q_e = K_F C_e^{1/n_F} \quad (4)$$

where  $K_F$  is the Freundlich adsorption constant ((mg g<sup>-1</sup>)(mg L<sup>-1</sup>)<sup>-n</sup>), and  $n_F$  is the Freundlich exponent coefficient. The value of  $1/n_F$  can be used to predict the favourability of the adsorption process, that is when  $1/n_F < 1$ .

Three-parameter isotherm model was also applied for fitting equilibrium data, which is the Redlich-Peterson model. The Redlich-Peterson model represents a combination of Langmuir and Freundlich isotherms for predicting the homogeneous approach to the surface area of the adsorbent [36]. The hyperbolic model of the Redlich-Peterson isotherm is given in Eq. (5):

$$Q_e = \frac{A_{RP} C_e}{1 + B_{RP} C_e^{\beta_{RP}}} \quad (5)$$

where  $A_{RP}$  and  $B_{RP}$  are the Redlich-Peterson isotherm parameters with the unit of L g<sup>-1</sup> and L mg<sup>-1</sup>, respectively. The exponential coefficient  $\beta_{RP}$  usually has a value in the range of 0 to 1, which provides the prediction of the homogeneity of the adsorbate.

The plots showing the adsorption isotherms of BB9 on Alg, Alg/RCE, and Alg/GA/RCE at different temperatures are given in Fig. 6. In all cases, the isotherm plots reflect an *L*-curve subclass 2 according to the classification by Giles et al. The *L*-curve is often observed for the solute adsorption in an aqueous solution where the adsorption process proceeds until the number of adsorption sites becomes depleted, and the adsorbent is finally saturated with solute molecules. In addition, the plateau in the adsorption system belonging to subclass 2 occurs due to the adsorbent monolayer saturation. Thus, it also implies that the adsorbents with a higher number of adsorption sites possess a greater adsorption capacity. This premise is reasonable to explain the higher adsorption capacity of Alg/GA/RCE than Alg and Alg/RCE. The higher number of adsorption sites in the Alg/GA/RCE surface can be attributed to the crosslinking of the polyphenols in the Alg matrix by GA.

The fitted parameters of the BB9 equilibrium adsorption data using Langmuir, Freundlich, and Redlich-Peterson models are presented in Table 1. The Langmuir and Redlich-Peterson models seem to fit the adsorption data better than the Freundlich model, judging from the correlation coefficient  $R^2$  (which is close to 1) and the low root-mean-square error (RMSE) values. The Redlich-Peterson is a hybrid model of Langmuir and Freundlich, where the value of  $\beta_{RP}$  parameter can describe the tendency of the adsorption system. As the value of  $\beta_{RP}$  close to 0, a heterogeneous adsorption system is obtained as the Redlich-Peterson equation is reduced to the Freundlich equation. On the contrary, as  $\beta_{RP}$  close to 1, this equation is reduced to Langmuir, and thereby homogeneous adsorption behavior is expected. Table 1 shows that the  $\beta_{RP}$  value is close to 1 for almost all systems, implying that the adsorption approaches the Langmuir model. The fitting results are also consistent with the previous classification by Giles et al., where most of the adsorption systems with an *L*-curve are well-convergence with the Langmuir model fitting [37]. The satisfactory fitting of the adsorption data to the Langmuir model is also an indicative that the dye molecules are adsorbed flat on the surface of the adsorbent.

The adsorption process of BB9 onto the BHB particles seems to be temperature-dependent. A higher adsorption capacity is achieved at elevated temperatures of the system. This phenomenon can be explained by the solubility nature of the solute dye molecules (i.e., BB9). The solubility of the adsorbate will be higher as the temperature increases, thus facilitating its mobility toward the adsorbent matrix. Moreover, an increase in temperature may also induce a greater swelling degree of the BHB, which could promote the pore enlargement of the adsorbent and facilitate the diffusion of the dye molecules into the adsorption sites.

The fit parameter of the Langmuir model, that is  $Q_{L,\max}$ , shows that Alg/GA/RCE has the highest monolayer adsorption capacity than Alg and Alg/RCE across all temperatures; suggesting that the crosslinking of RCE polyphenols into the Alg matrix resulted in the significant improvement in the adsorption capacity. This performance improvement can be attributed to the presence of RCE polyphenols that provide additional adsorption sites for cationic dye molecules in the form of functional groups such as -OH, -OCH<sub>3</sub>, and -COOH. The as-prepared Alg/GA/RCE also shows superior adsorption capacity toward BB9 compared to other previously reported alginate-based composite adsorbents, as listed in Table 2. It is worth noting that Alg/GA/RCE possesses higher adsorption capacity toward BB9 than the mentioned Alg-based adsorbents and the common adsorbents (i.e., activated carbon and clay mineral). However, in a recyclability test attempt, the BHB particles broke after the first reuse experiment due to excessive swelling, thus indicating that this adsorbent is unlikely to be recycled. However, BHB offers several advantages, such as high adsorption capacity, low

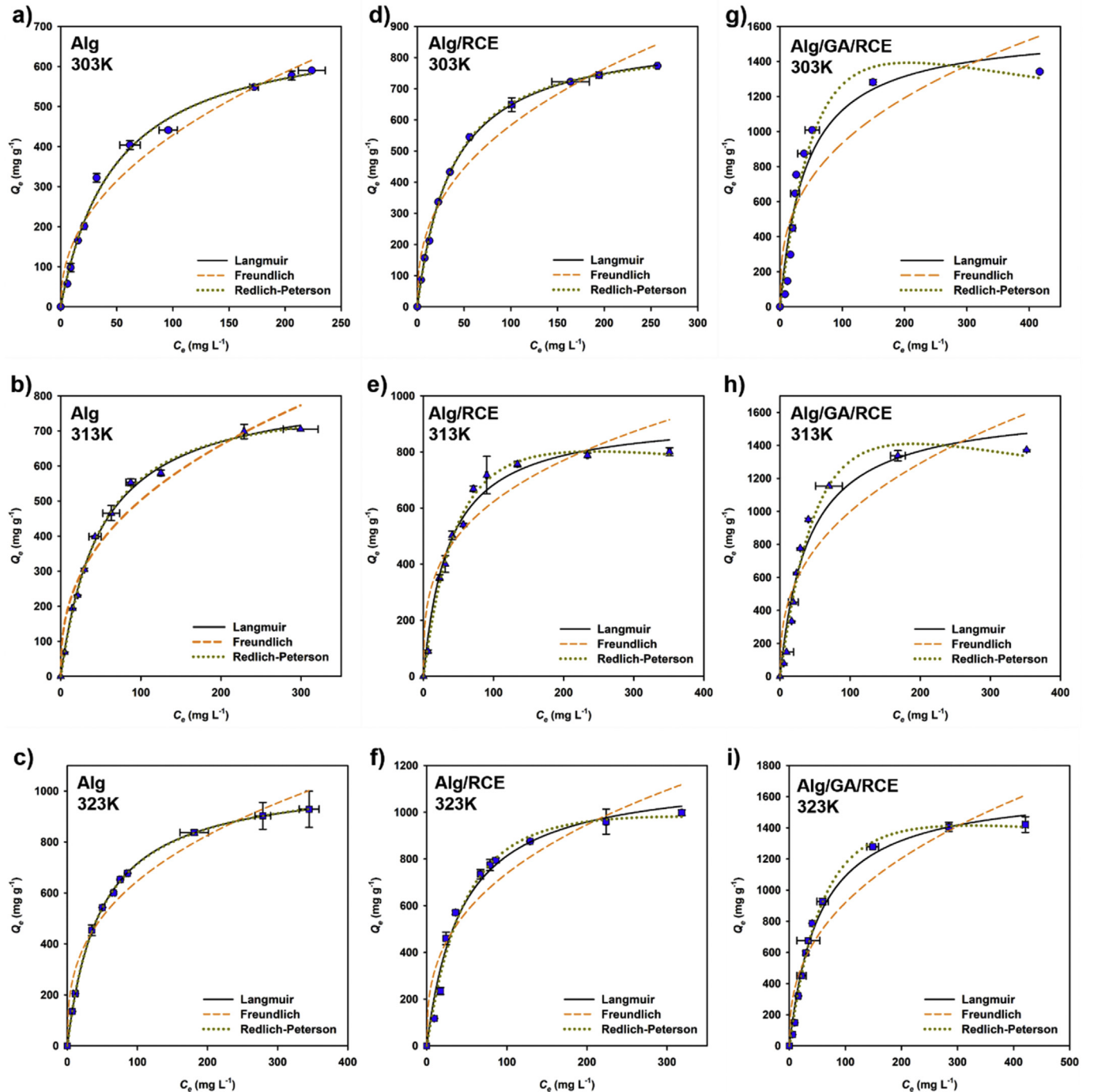


**Fig. 6.** Adsorption isotherm data at different temperatures and the nonlinear fittings using Langmuir, Freundlich, and Redlich-Peterson models.

cost, and ease of preparation. Also, BHB is prepared from non-toxic, naturally abundant, and environmentally benign materials, which are expected not to cause environmental damage when disposed-of.

#### 3.4. Adsorption kinetics

The adsorption kinetics of BB9 onto BHB (i.e., Alg/, Alg/RCE, and Alg/GA/RCE) were studied at the optimal pH of 11 and 30 °C. The adsorption kinetics data were interpreted using the pseudo 1st order, pseudo 2nd order, and Elovich model. The nonlinear mathematical equations for pseudo 1st order and pseudo 2nd order are presented in Eqs. (6) and (7), respectively [46].

$$Q_t = Q_1 \left( 1 - e^{-k_1 t} \right) \quad (6)$$

$$Q_t = \frac{k_2 Q_2^2 t}{1 + k_2 Q_2 t} \quad (7)$$

where \$Q\_t\$ (mg g\$^{-1}\$) represents the amount of BB9 adsorbed at a specified time \$t\$ (h). \$Q\_1\$ (mg g\$^{-1}\$) and \$Q\_2\$ (mg g\$^{-1}\$) are the estimated equilibrium amount of BB9 adsorbed for pseudo 1st and pseudo 2nd order rate equations, respectively. The parameter \$k\_1\$ (h\$^{-1}\$) and \$k\_2\$ (g mg\$^{-1}\$ h\$^{-1}\$) are the corresponding apparent sorption rate constant of pseudo 1st and pseudo 2nd kinetic models, respectively.

**Table 1**

Adsorption isotherm parameters for the adsorption of BB9 on BHB (Alg, Alg/RCE, and Alg/GA/RCE) at different temperatures.

Model	Parameter	Alg	Alg/RCE	Alg/GA/RCE
Adsorption at $T = 303\text{ K}$				
Langmuir	$Q_{L,\max} (\text{mg g}^{-1})$	725	886	1389
	$K_L (\text{L mg}^{-1})$	0.02	0.03	0.02
	$R^2$	0.99	1.00	0.92
	RMSE	19.31	7.13	31.85
Freundlich	$K_F (\text{mg g}^{-1}) (\text{mg L}^{-1})^{1/n}$	54.28	96.54	184.34
	$n_F$	0.45	0.39	0.3525
	$R^2$	0.97	0.96	0.80
	RMSE	41.69	57.90	48.48
Redlich-Peterson	$Q_{RP} (\text{mg g}^{-1})$	809	1084	1418
	$\beta_{RP}$	1.00	1.03	1.11
	$R^2$	0.99	1.00	0.95
	RMSE	20.48	6.62	62.57
Adsorption at $T = 313\text{ K}$				
Langmuir	$Q_{L,\max} (\text{mg g}^{-1})$	840	921	1400
	$K_L (\text{L mg}^{-1})$	0.02	0.03	0.03
	$R^2$	1.00	0.98	0.95
	RMSE	12.86	37.47	45.68
Freundlich	$K_F (\text{mg g}^{-1}) (\text{mg L}^{-1})^{1/n}$	82.34	151.75	180.73
	$n_F$	0.40	0.31	0.37
	$R^2$	0.97	0.90	0.84
	RMSE	12.86	94.31	54.84
Redlich-Peterson	$Q_{RP} (\text{mg g}^{-1})$	923	1206	1489
	$\beta_{RP}$	1.05	1.22	1.13
	$R^2$	1.00	0.99	0.98
	RMSE	12.87	23.55	49.00
Adsorption at $T = 323\text{ K}$				
Langmuir	$Q_{L,\max} (\text{mg g}^{-1})$	1055	1169	1442
	$K_L (\text{L mg}^{-1})$	0.021	0.02	0.03
	$R^2$	0.98	0.98	0.99
	RMSE	29.54	50.61	23.19
Freundlich	$K_F (\text{mg g}^{-1}) (\text{mg L}^{-1})^{1/n}$	92.78	141.41	123.39
	$n_F$	0.34	0.36	0.45
	$R^2$	0.89	0.91	0.92
	RMSE	46.40	112.62	47.59
Redlich-Peterson	$Q_{RP} (\text{mg g}^{-1})$	968	1261	1567
	$\beta_{RP}$	1.02	1.16	1.17
	$R^2$	0.99	0.98	1.00
	RMSE	22.60	44.82	28.50

The Elovich model is postulated to suit the chemical adsorption systems with heterogeneous adsorbent surfaces, which has the following expression:

$$Q_t = \frac{1}{\beta} \ln(1 + \alpha\beta t) \quad (8)$$

where  $\alpha (\text{mg g}^{-1} \text{ h}^{-1})$  is the initial adsorption rate and  $\beta (\text{g mg}^{-1})$  is the desorption constant. An equilibrium constant ( $R_E$ ) representing the adsorption characteristic can be calculated from the Elovich parameters:

$$R_E = 1/Q_{ref}\beta \quad (9)$$

with  $Q_{ref}$  is the adsorption capacity obtained at  $t = t_{ref}$  and  $t_{ref}$  is the longest time in adsorption process. The adsorption characteristics based on  $R_E$  can be classified as follows: slow rising when  $R_E > 0.3$ , mild rising for  $0.3 > R_E > 0.1$ , rapid rising for  $0.1 > R_E > 0.02$ , and instantaneous approaching equilibrium when  $R_E < 0.02$  [47,48].

The fitting of the kinetic models to the experimental data is presented in Fig. 7, while the values of the fit parameters are given in Table 3. Among the three investigated kinetic equations, the pseudo 1st order was the most suitable model to fit the data points for BB9 adsorption by BHB (Alg, Alg/RCE, and Alg/GA/RCE). This suitability can be observed from the correlation factor values ( $R^2$ ) of the Pseudo 1st order, which approach unity. Also, the low RMSE of the Pseudo 1st order further confirms the suitability of the model. When an adsorption

**Table 2**

Maximum adsorption capacity of BB9 on several Alg-based composite adsorbents.

Adsorbent <sup>a</sup>	$Q_{L,\max} (\text{mg g}^{-1})$	Ref
GO/Alg	357.14	[38]
PVA/Alg/Chitosan/Mont	137.15	[39]
TA/PVA/Alg	147.09	[40]
Alg/Rice husk	344.00	[41]
GO-Mont/Alg	150.66	[42]
Hectorite/Alg	785.45	[43]
Activated carbon (from <i>Camellia sinensis</i> L.)	324.7	[44]
Activated clay minerals	500	[45]
Biocomposite Hydrogel Beads (Alg/GA/RCE)	1442	This work

<sup>a</sup> GO = graphene oxide, Alg = sodium alginate, PVA = poly(vinyl alcohol), Mont = montmorillonite, TA = tannic acid.

system fits the Pseudo 1st order, it can be implied that the rate constant ( $k_1$ ) of the system is dependent on the initial concentration of the solute ( $C_0$ ) [46]. As shown in Table 3, the dependency of  $k_1$  to  $C_0$  can be clearly observed from the difference of  $k_1$  values for each system with different  $C_0$ .

Furthermore, it can be observed that while the values of  $Q_t$  increase with increasing  $C_0$ ,  $k_1$  decreased with increasing  $C_0$ . This can be related to the relation between the mass transfer driving force and  $C_0$ . At high  $C_0$ , the high number of solute molecules cause an increased mass transfer rate toward the adsorbent surface; thus providing a larger driving force for the solute to overcome the adsorbent boundary layer, and consequently a higher number of solute molecules can be adsorbed. However, a high number of solute molecules also cause the external surface vacant sites of the adsorbent are quickly occupied and thus slow down the diffusion rate of the remaining solute molecules in the bulk solution [46,49]. Once all of the surface sites are occupied, the next adsorption step occurs through the diffusion of the solute molecules into the interior porous adsorbent matrix [49].

Fig. 7 also shows the gradual increase in  $Q_t$  over a prolonged time until it reaches a plateau condition. In the first couple of hours (~3 h), a rapid increase in  $Q_t$  was observed, and subsequently there is no significant increase in  $Q_t$  after 3 h. This phenomenon can be directly attributed to the high availability of vacant adsorption sites at the initial stage. With prolonged adsorption time, the vacant sites become gradually occupied and finally saturated with the solute molecules, thus leading to the saturation of  $Q_t$  [50].

By comparing the three investigated BHB sorbents, Alg/GA/RCE displays the highest adsorption capacity ( $Q_1$ ) than Alg/RCE and Alg. This result indicates the promoting effect of the RCE addition to the adsorption capacity of the Alg. Interestingly, although the amount of BB9 adsorbed on Alg was lower than Alg/GA/RCE, the adsorption rate ( $k_1$ ) was slightly higher for Alg. This may be attributed to the higher number of adsorption sites in Alg/GA/RCE; thus, a longer time is needed to occupy all of the available sites.

Although the kinetic data can be well described by the Pseudo 1st model, it is still interesting to examine the fit parameters from other models. The calculated parameters  $Q_2$  in the Pseudo 2nd order model shows higher values for Alg/GA/RCE than Alg/RCE and Alg, which display good consistency with the  $Q_1$  parameter of the Pseudo 1st order. The fitting of the kinetic data using the Elovich model shows lower congruity than other fitting models. This may suggest that the chemisorption is not dominant in this process. Furthermore, as shown from the  $\alpha$  value, the initial adsorption rate was higher at higher initial adsorbate concentrations, which implies that higher adsorbate concentrations provide a greater mass transfer driving force for the adsorption. Meanwhile, desorption of the adsorbate was higher at a lower concentration, as reflected by the high  $\beta$  value. Based on the  $R_E$  value, a slow rising characteristic was observed at high  $C_0$ , and it altered to mild-rapid rising characteristics at low  $C_0$ . This result is in accordance with the adsorption rate constants  $k_1$  and  $k_2$ , which show lower values with increasing  $C_0$  parameter.

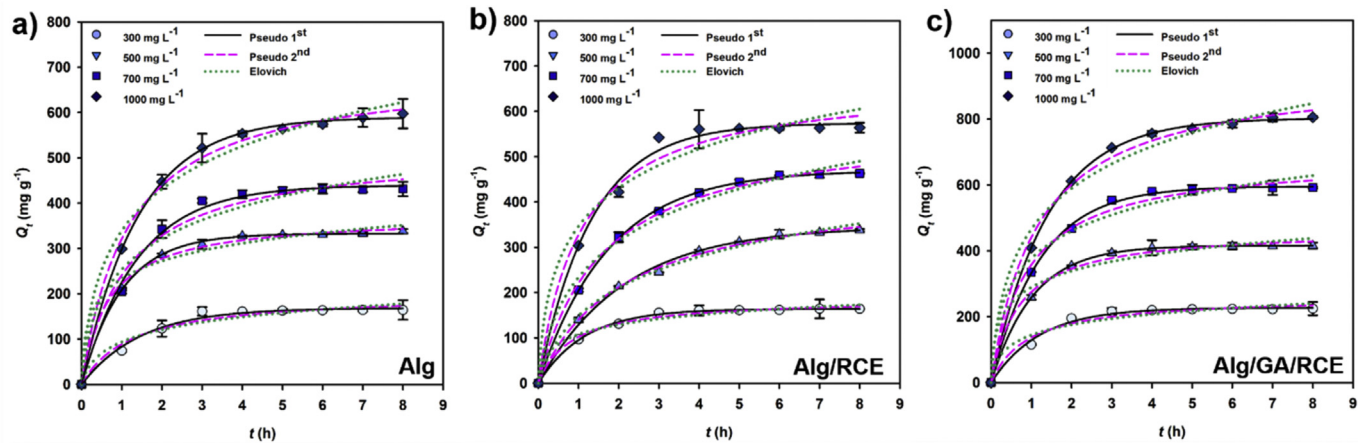


**Fig. 7.** Adsorption kinetics of BB9 on BHB at various initial concentrations, and the kinetic data fitting using Pseudo 1st order, Pseudo 2nd order, and Elovich model.

### 3.5. Intraparticle diffusion (IPD) behavior

The initial rapid adsorption behavior of the BB9 on BHB was further analyzed by fitting the kinetic data using the IPD model. The IPD equation can be expressed as follows:

$$Q_t = k_{\text{IPD}} t^{1/2} + C_i \quad (10)$$

where  $k_{\text{IPD}}$  ( $\text{mg g}^{-1} \text{h}^{-1/2}$ ) is the intraparticle diffusion rate constant and  $C_i$  ( $\text{mg g}^{-1}$ ) is the arbitrary constant. The  $C_i$  value is postulated to be closely related to the boundary layer effect, where the greater the value, the greater the boundary. The IPD model has three forms according to the method of data fitting: (1) by fitting a straight line that is forced to pass through the origin, (2) by fitting two or three segments straight line, which is known as a multi-linearity plot, and (3) by fitting a straight line that is not necessarily pass through the origin [46,49,50]. The kinetic data fitting using the single straight line of the IPD model results in a poor  $R^2$  value (<0.90), which implies the inadequacy of this fitting approach to interpret the kinetic data. Thus, the multi-linearity approach is applied for the data fitting [51].

The IPD fitting onto the adsorption kinetics data of BB9 on three BHB adsorbents can be divided into two segments for all  $C_0$  variants. The first segment ranged from 1 to 4 h (1 to  $2 \text{ h}^{1/2}$ ) of contact time, and the

second segment ranged from 4 to 8 h (2 to  $2.83 \text{ h}^{1/2}$ ) of contact time (See Fig. 8). The first segment corresponds to the instantaneous (rapid) surface adsorption, which is confirmed by the high diffusion rate  $k_{\text{IPD},1}$ . The second segment can be assigned to the gradual adsorption step where intraparticle (or pore) diffusion occurs; thus, this segment has a lower rate constant ( $k_{\text{IPD},2}$ ). The lower values of  $k_{\text{IPD},2}$  could also be ascribed to the larger boundary layer effect (see Table 4), which is larger for the second segment compared to the first segment ( $C_{i,2} > C_{i,1}$ ) [51,52]. A similar result was obtained in the study by Tiwari et al. (2016), where the adsorption system of lead by the composite of Alg/magnetite nanoparticles/bacterial strain followed the two-segment IPD characteristic [53].

### 3.6. Thermodynamic evaluation

Thermodynamic parameters of adsorption, such as the Gibbs free energy change ( $\Delta G$ ), enthalpy change ( $\Delta H$ ), and entropy change ( $\Delta S$ ), are the relevant parameters describing the spontaneity and the characteristic of the adsorption process [54]. The thermodynamic parameters at a constant temperature and pressure are calculated according to the following equations:

$$\Delta G = \Delta H - T \cdot \Delta S \quad (11)$$

**Table 3**  
Adsorption kinetics parameters for the adsorption of BB9 on BHB.

Model	$C_0$ ( $\text{mg L}^{-1}$ )											
	Alg				Alg/RCE				Alg/GA/RCE			
	300	500	700	1000	300	500	700	1000	300	500	700	1000
Pseudo 1st order												
$Q_1$ ( $\text{mg g}^{-1}$ )	168	383	439	590	164	345	470	674	226	416	595	803
$k_1$ ( $\text{h}^{-1}$ )	1.09	1.01	0.74	0.71	0.87	0.85	0.77	0.60	0.84	0.82	0.73	0.71
$R^2$	0.99	1.00	1.00	1.00	1.00	1.00	1.00	0.99	1.00	1.00	1.00	1.00
RMSE	6.86	3.51	11.00	5.76	2.39	7.64	3.19	15.96	4.11	6.39	5.72	1.05
Pseudo 2nd order												
$Q_2$ ( $\text{mg g}^{-1}$ )	200	372	518	696	186	437	617	667	261	466	684	944
$k_2$ ( $\text{g mg}^{-1} \text{h}^{-1}$ )	0.004	0.004	0.002	0.001	0.004	0.003	0.001	0.002	0.004	0.003	0.002	0.001
$R^2$	0.97	1.00	0.98	1.00	0.99	1.00	1.00	0.98	0.98	0.99	0.99	1.00
RMSE	10.69	7.38	22.17	14.09	5.18	6.63	10.45	27.01	11.82	19.34	20.62	7.32
Elovich												
$\alpha$ ( $\text{mg g}^{-1} \text{h}^{-1}$ )	875	968	970	1415	914	913	1033	1791	968	1767	1784	2003
$\beta$ ( $\text{g mg}^{-1}$ )	0.023	0.018	0.010	0.007	0.031	0.009	0.008	0.008	0.021	0.014	0.008	0.005
$R_E$	0.16	0.17	0.24	0.34	0.19	0.33	0.29	0.33	0.06	0.12	0.30	0.58
$R^2$	0.94	0.98	0.96	0.98	0.98	0.99	0.99	0.96	0.95	0.98	0.97	0.98
RMSE	14.01	14.36	31.51	26.25	8.50	9.79	19.26	37.91	17.84	20.82	31.92	37.54

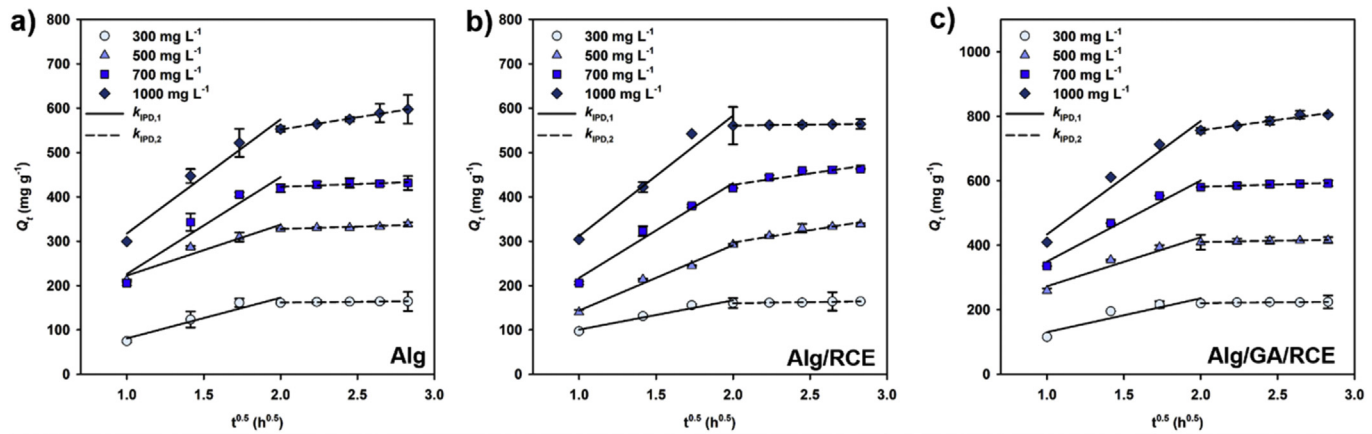


**Fig. 8.** Adsorption kinetics of BB9 on BHB at various initial concentrations and the data fitting using the intraparticle diffusion (IPD) model.

**Table 4**

Calculated IPD parameters for the adsorption of BB9 on BHB.

$C_0$ (mg L <sup>-1</sup> )	$k_{IPD,1}$ (mg g <sup>-1</sup> h <sup>-1/2</sup> )	$C_{i,1}$ (mg g <sup>-1</sup> )	$R^2$	RMSE	$k_{IPD,2}$ (mg g <sup>-1</sup> h <sup>-1/2</sup> )	$C_{i,2}$ (mg g <sup>-1</sup> )	$R^2$	RMSE
<b>Alg</b>								
300	91.76	11.06	0.93	13.58	3.76	153.91	0.87	0.55
500	114.74	107.58	0.94	15.15	10.76	305.88	0.82	1.91
700	218.73	97.19	0.93	32.39	12.66	397.44	0.80	3.21
1000	259.92	257.43	0.96	28.15	54.80	442.62	0.99	1.64
<b>Alg/RCE</b>								
300	66.06	34.46	0.96	7.19	4.91	150.31	0.88	0.70
500	147.45	93.93	0.99	8.55	5.23	186.65	0.92	6.11
700	214.17	102.89	0.98	16.90	5.82	325.92	0.85	8.09
1000	271.93	139.47	0.96	28.29	54.34	552.19	0.98	0.22
<b>Alg/GA/RCE</b>								
300	101.32	28.46	0.90	28.55	4.96	210.66	0.94	0.74
500	151.66	121.05	0.97	20.93	7.93	394.11	0.92	0.87
700	251.68	97.65	0.94	25.02	14.83	551.60	0.97	1.48
1000	351.73	81.87	0.96	38.46	64.40	627.95	0.96	4.78

$$\Delta G = -RT \ln K \quad (12)$$

where  $\Delta G$  represents the Gibbs free energy (kJ mol<sup>-1</sup>) and  $K$  is the equilibrium constant, which can also be related to the equilibrium adsorption capacity expressed as  $\ln(Q_e/C_e)$ ;  $R$  is the universal gas constant (8.314 J mol<sup>-1</sup> K<sup>-1</sup>). Thus, Eq. (11) can be rearranged to the following expression:

$$\ln \frac{Q_e}{C_e} = \frac{-\Delta H}{RT} + \frac{\Delta S}{R} \quad (13)$$

The values of  $\Delta H$  and  $\Delta S$  can be obtained as the slope and intercept of the Van't Hoff plot  $\ln(Q_e/C_e)$  vs.  $1/T$ , respectively. The calculated thermodynamic parameters are given in Table 5.

As can be seen in Table 5, the negative values of  $\Delta G$  indicate that the adsorption proceeds spontaneously. Also, the more negative values of  $\Delta G$  imply that the adsorption is more spontaneous at higher temperatures. Meanwhile, the positive value of  $\Delta H$  reflects an endothermic nature of the adsorption process, and thus, adsorption is more favorable at high temperatures. Moreover, the  $\Delta H$  value of <20 kJ mol<sup>-1</sup> suggests that physisorption is more dominant in the BB9 uptake process onto BHB and that the adsorption occurs mainly due to the van der Waals forces [37]. The positive value of  $\Delta S$  suggests increased randomness at the solid-liquid interface, leading to decreased solution viscosity. The decrease in viscosity allows an increase in the mass transfer driving force of the solute molecules, which facilitates adsorption.

### 3.7. Cost analysis

The preliminary analysis of the direct operating cost (DOC) was conducted to estimate the production cost of the Alg/GA/RCE hydrogel beads. In this context, the production of Alg/GA/RCE only involved a mixing process of all precursor materials and did not require any complicated procedure and a large number of workers. Therefore, the DOC analysis of the production of Alg/GA/RCE is calculated based on the costs of the raw materials, and the contribution of utility and operating

**Table 5**  
Thermodynamic parameters of the BB9 adsorption on BHB sorbents.

$T$ (K)	$\Delta G$ (kJ mol <sup>-1</sup> )	$\Delta H$ (kJ mol <sup>-1</sup> )	$\Delta S$ (kJ mol <sup>-1</sup> K <sup>-1</sup> )
<b>Alg</b>			
303	-1.9124	9.4163	0.0373
313	-2.2283		
323	-2.6589		
<b>Alg/RCE</b>			
303	-2.4536	16.524	0.0756
313	-3.0193		
323	-3.9661		
<b>Alg/GA/RCE</b>			
303	-3.3627	18.7539	0.0729
313	-3.8902		
323	-4.5255		

**Table 6**

Estimation of DOC for the synthesis of Alg/GA/RCE on the kilogram scale.

DOC	Specification	Price (US\$ kg <sup>-1</sup> ) <sup>a</sup>	Amount (kg) <sup>b</sup>	Total (US\$)
Alg	Mw 10,000–600,000	4.00	0.06	0.240
CaCl <sub>2</sub>	Flakes, 74%	0.12	0.03	0.041
GA	50%	10.0	0.004	0.040
H <sub>2</sub> O	18.2 MΩ	0.05	3.0	0.150
Ethanol	Min. 96%	0.95	2.5	2.375
Acetic acid	Glacial, 99.5%	0.41	0.004	0.002
Red cabbage	–	0.12	3.0	0.360
Total DOC				3.170

<sup>a</sup> The raw materials price was based on the China trading price listed by Focus Technology Co. Ltd.

<sup>b</sup> The amount of the raw materials was scaled up on the basis of one kilogram of dried beads production. The estimated amount of water includes water requirements in the beads production process and the washing step.

labor costs can be neglected. The price of the raw materials along with their price quotes in US\$ are presented in Table 6. The production of Alg/GA/RCE costs only US\$3.17 per kg, which is comparable to or even cheaper than other commercial adsorbent materials such as activated carbons (US\$0.75–2.60 per kg), bentonite clays (US\$0.5–2.2 per kg), silica gels (US\$4.4–5.3 per kg), and polymer beads (US\$5.5 per kg). Furthermore, it is worth mentioning that the adsorption capacity of Alg/GA/RCE hydrogel beads is superior to those of activated carbons and clay minerals (see Table 2), thus implying the application potential of this low-cost alternative adsorbent for dye wastewater treatment.

## 4. Conclusions

The present study demonstrates a facile and green approach for enhancing the adsorption capacity of Alg-based hydrogel adsorbent by crosslinking phytochemicals (i.e., phenolics, anthocyanin, and flavonoids) from RCE using glutaraldehyde. The resulting Alg/GA/RCE BHB exhibits a maximum adsorption capacity of 1442 mg g<sup>-1</sup> toward BB9 dye cations, which is higher than other Alg-based composite adsorbents. The adsorption study shows that the adsorption was dominated by physisorption, and the adsorption occurs due to the van der Waals interaction. The rapid and instantaneous adsorption occurred at the beginning of the process and continued by the intraparticle diffusion process. The adsorption isotherm and kinetics parameters show good agreement with the thermodynamic parameters. In summary, the as-prepared Alg/GA/RCE BHB can be potentially employed as a single-use adsorbent to purify dye-contaminated wastewater with excellent adsorption performance.

## Declaration of Competing Interest

The authors declare that they have no known competing financial interests or personal relationships that could have appeared to influence the work reported in this paper.

## Acknowledgements

The authors gratefully acknowledge financial support from the Widya Mandala Surabaya Catholic University through Internal Research Grant.

## References

- K.K. Samanta, P. Pandit, P. Samanta, S. Basak, Water consumption in textile processing and sustainable approaches for its conservation, in: S.S. Muthu (Ed.), *Water in Textiles and Apparel: Consumption, Footprint, and Life Cycle Assessment*, Elsevier, Woodhead Publishing 2019, pp. 41–59.
- J.H. Beh, T.H. Lim, J.H. Lew, J.C. Lai, Cellulose nanofibril-based aerogel derived from sago pith waste and its application on methylene blue removal, *Int. J. Biol. Macromol.* 160 (2020) 836–845, <https://doi.org/10.1016/j.ijbiomac.2020.05.227>.
- C.I. Pearce, J.R. Lloyd, J.T. Guthrie, The removal of colour from textile wastewater using whole bacterial cells: a review, *Dyes Pigments* 58 (2003) 179–196, [https://doi.org/10.1016/S0143-7208\(03\)00064-0](https://doi.org/10.1016/S0143-7208(03)00064-0).
- U. Meyer, Biodegradation of synthetic organic colorants, *FEMS Symp.* 12 (1981) 371–385.
- J. Panigrahi, S.C. Sharma, Simulation, control, and optimization of water systems in industrial plants, in: V.V. Ranade, V.M. Bhandari (Eds.), *Industrial Wastewater Treatment, Recycling and Reuse*, Butterworth-Heinemann 2014, pp. 463–487.
- T. Robinson, C. McMullan, R. Marchant, P. Nigam, Remediation of dyes in textile effluent: a critical review on current treatment technologies with a proposed alternative, *Bioresour. Technol.* 77 (2001) 247–255, [https://doi.org/10.1016/S0960-8524\(00\)00080-8](https://doi.org/10.1016/S0960-8524(00)00080-8).
- S.P. Glaeser, B.A. Berghoff, V. Stratmann, H.-P. Grossart, J. Glaeser, Contrasting effects of singlet oxygen and hydrogen peroxide on bacterial community composition in a humic lake, *PLoS One* 9 (2014), e92518, <https://doi.org/10.1371/journal.pone.0092518>.
- E. Santoso, R. Ediaty, Y. Kusumawati, H. Bahruji, D.O. Sulistiono, D. Prasetyoko, Review on recent advances of carbon based adsorbent for methylene blue removal from waste water, *Mater. Today Chem.* 16 (2020) 100233, <https://doi.org/10.1016/j.mtchem.2019.100233>.
- O.S. Bayomie, H. Kandeel, T. Shoeib, H. Yang, N. Youssef, M.M.H. El-Sayed, Novel approach for effective removal of methylene blue dye from water using fava bean peel waste, *Sci. Rep.* 10 (2020) 7824, <https://doi.org/10.1038/s41598-020-64727-5>.
- N. Willmott, J. Guthrie, G. Nelson, The biotechnology approach to colour removal from textile effluent, *J. Soc. Dye. Colour.* 114 (1998) 38–41, <https://doi.org/10.1111/j.1478-4408.1998.tb01943.x>.
- G. Fadillah, T.A. Saleh, S. Wahyuningsih, E. Ninda Karina Putri, S. Febrianastuti, Electrochemical removal of methylene blue using alginate-modified graphene adsorbents, *Chem. Eng. J.* 378 (2019), 122140, <https://doi.org/10.1016/j.cej.2019.122140>.
- S.P. Santoso, L. Laysandra, J.N. Putro, J. Lie, F.E. Soetaredjo, S. Ismadji, A. Ayucitra, Y.H. Ju, Preparation of nanocrystalline cellulose-montmorillonite composite via thermal radiation for liquid-phase adsorption, *J. Mol. Liq.* 233 (2017) 29–37, <https://doi.org/10.1016/j.molliq.2017.02.091>.
- W.S. Tan, A.S.Y. Ting, Alginate-immobilized bentonite clay: adsorption efficacy and reusability for Cu(II) removal from aqueous solution, *Bioresour. Technol.* 160 (2014) 115–118, <https://doi.org/10.1016/j.biortech.2013.12.056>.
- R. Fabryanty, C. Valencia, F.E. Soetaredjo, J.N. Putro, S.P. Santoso, A. Kurniawan, Y.-H. Ju, S. Ismadji, Removal of crystal violet dye by adsorption using bentonite – alginate composite, *J. Environ. Chem. Eng.* 5 (2017) 5.
- L.M. Pandey Ravi, Enhanced adsorption capacity of designed bentonite and alginate beads for the effective removal of methylene blue, *Appl. Clay Sci.* 169 (2019) 102–111, <https://doi.org/10.1016/j.clay.2018.12.019>.
- J.H. Chen, J.C. Ni, Q.L. Liu, S.X. Li, Adsorption behavior of cd(II) ions on humic acid-immobilized sodium alginate and hydroxyl ethyl cellulose blending porous composite membrane adsorbent, *Desalination* 285 (2012) 54–61, <https://doi.org/10.1016/j.desal.2011.09.033>.
- H.E. Khoo, A. Azlan, S.T. Tang, S.M. Lim, Anthocyanidins and anthocyanins: colored pigments as food, pharmaceutical ingredients, and the potential health benefits, *Food Nutr. Res.* 61 (2017) 3.
- A. Hosu, V.-M. Cristea, C. Cimpoiu, Analysis of total phenolic, flavonoids, anthocyanins and tannins content in Romanian red wines: prediction of antioxidant activities and classification of wines using artificial neural networks, *Food Chem.* 150 (2014) 113–118, <https://doi.org/10.1016/j.foodchem.2013.10.153>.
- J.J.M. Órfão, A.I.M. Silva, J.C.V. Pereira, S.A. Barata, I.M. Fonseca, P.C.C. Faria, M.F.R. Pereira, Adsorption of a reactive dye on chemically modified activated carbons–influence of pH, *J. Colloid Interface Sci.* 296 (2006) 480–489, <https://doi.org/10.1016/j.jcis.2005.09.063>.
- B. Kusukham, J. Prasertgul, P. Srimun, Morphology and property of calcium silicate encapsulated with alginate beads, *Silicon* 6 (2014) 191–197, <https://doi.org/10.1007/s12633-013-9173-z>.
- C.R. Badita, D. Aranghel, C. Burducea, P. Mereuta, Characterization of sodium alginate based films, *Rom. J. Phys.* 65 (2020) 602.
- P. Sundarajan, P. Eswaran, A. Marimuthu, L.B. Subhadra, P. Kannaiyan, One pot synthesis and characterization of alginate stabilized semiconductor nanoparticles, *Bull. Kor. Chem. Soc.* 33 (2012) 3218–3224, <https://doi.org/10.5012/bkcs.2012.33.10.3218>.
- O. Bayraktar, I. Erdoğan, M.D. Köse, G. Kalmaç, Nanocarriers for plant-derived natural compounds, in: A. Ficai, A.M. Grumezescu (Eds.), *Micro and Nano Technologies*, Elsevier 2017, pp. 395–412.
- P. Rijo, D. Matias, A.S. Fernandes, M.F. Simões, M. Nicolai, C.P. Reis, Antimicrobial plant extracts encapsulated into polymeric beads for potential application on the skin, *Polymers* 6 (2014) 479–490, <https://doi.org/10.3390/polym6020479>.
- W. Zam, G. Bashour, W. Abdelwahed, W. Khayata, Alginate–pomegranate peels’ polyphenols beads: effects of formulation parameters on loading efficiency, *Braz. J. Pharm. Sci.* 50 (2014) 741–748, <https://doi.org/10.1590/S1984-82502014000400009>.
- S.P. Santoso, A. Kurniawan, F.E. Soetaredjo, K.-C. Cheng, J.N. Putro, S. Ismadji, Y.-H. Ju, Eco-friendly cellulose–bentonite porous composite hydrogels for adsorptive removal of azo dye and soilless culture, *Cellulose* 26 (2019) 3339–3358, <https://doi.org/10.1007/s10570-019-02314-2>.
- A. Kurniawan, H. Sutiono, N. Indraswati, S. Ismadji, Removal of basic dyes in binary system by adsorption using rarasaponin–bentonite: revisited of extended Langmuir

- model, Chem. Eng. J. 189–190 (2012) 264–274, <https://doi.org/10.1016/j.cej.2012.02.070>.
- [28] A.E. Angkawijaya, S.P. Santoso, V. Bundjaja, F.E. Soetaredjo, C. Gunarto, A. Ayucitra, Y.-H. Ju, A.W. Go, S. Ismadji, Studies on the performance of bentonite and its composite as phosphate adsorbent and phosphate supplementation for plant, J. Hazard. Mater. 399 (2020) 123130, <https://doi.org/10.1016/j.jhazmat.2020.123130>.
- [29] J.J. Salazar-Rabago, R. Leyva-Ramos, J. Rivera-Utrilla, R. Ocampo-Perez, F.J. Cerino-Cordova, Biosorption mechanism of methylene blue from aqueous solution onto white pine (*Pinus durangensis*) sawdust: effect of operating conditions, Sustain. Environ. Res. 27 (2017) 32–40, <https://doi.org/10.1016/j.serj.2016.11.009>.
- [30] A. Benhouria, M.A. Islam, Z.-B. Hassina, M. Boutahala, B. Hameed, Calcium alginate-bentonite-activated carbon composite beads as highly effective adsorbent for methylene blue, Chem. Eng. J. 270 (2015) 621–630, <https://doi.org/10.1016/j.cej.2015.02.030>.
- [31] M. Friedman, H.S. Jürgens, Effect of pH on the stability of plant phenolic compounds, J. Agric. Food Chem. 48 (2000) 2101–2110, <https://doi.org/10.1021/jf990489j>.
- [32] S. Peng, L. Zou, W. Zhou, C. Liu, D.J. McClements, Encapsulation of lipophilic polyphenols into nanoliposomes using pH-driven method: advantages and disadvantages, J. Agric. Food Chem. 67 (2019) 7506–7511, <https://doi.org/10.1021/acs.jafc.9b01602>.
- [33] S.N. Pawar, K.J. Edgar, Alginate derivatization: a review of chemistry, properties and applications, Biomaterials 33 (2012) 3279–3305, <https://doi.org/10.1016/j.biomaterials.2012.01.007>.
- [34] I. Langmuir, The constitution and fundamental properties of solids and liquids, J. Am. Chem. Soc. 38 (1916) 2221–2295.
- [35] H.M.F. Freundlich, Over the adsorption in solution, J. Phys. Chem. 57 (1906) 385–470.
- [36] A. Nimibofa, A.N. Ebelegi, D. Wankasi, Modelling and interpretation of adsorption isotherms, J. Chem. NY 2017 (2017).
- [37] J.S. Piccin, T.R.S.A. Cadaval, L.A.A. de Pinto, G.L. Dotto, Adsorption isotherms in liquid phase: experimental, modeling, and interpretations, in: A. Bonilla-Petriciole, D.I. Mendoza-Castillo, H.E. Reynel-Ávila (Eds.), Adsorption Processes for Water Treatment and Purification, Springer International Publishing 2017, pp. 19–51.
- [38] X. Liu, B. Cui, S. Liu, Q. Ma, Methylene blue removal by graphene oxide/alginate gel beads, Fiber Polym. 20 (2019) 1666–1672, <https://doi.org/10.1007/s12221-019-9011-z>.
- [39] W. Wang, Y. Zhao, H. Bai, T. Zhang, V. Ibarra-Galvan, S. Song, Methylene blue removal from water using the hydrogel beads of poly(vinyl alcohol)-sodium alginate-chitosan-montmorillonite, Carbohydr. Polym. 198 (2018) 518–528, <https://doi.org/10.1016/j.carbpol.2018.06.124>.
- [40] T. Hu, Q. Liu, T. Gao, K. Dong, G. Wei, J. Yao, Facile preparation of tannic acid-poly (vinyl alcohol)/sodium alginate hydrogel beads for methylene blue removal from simulated solution, ACS Omega 3 (2018) 7523–7531, <https://doi.org/10.1021/acsomega.8b00577>.
- [41] E. Alver, A.Ü. Metin, F. Brouers, Methylene blue adsorption on magnetic alginate/rice husk bio-composite, Int. J. Biol. Macromol. 154 (2020) 104–113, <https://doi.org/10.1016/j.ijbiomac.2020.02.330>.
- [42] E. Tao, D. Ma, S. Yang, X. Hao, Graphene oxide-montmorillonite/sodium alginate aerogel beads for selective adsorption of methylene blue in wastewater, J. Alloys Compd. 832 (2020) 154833, <https://doi.org/10.1016/j.jallcom.2020.154833>.
- [43] R.R. Pawar, P. Lalhmunsima, S.Y. Gupta, B. Sawant, S.-M. Lee Shahmoradi, Porous synthetic hectorite clay-alginate composite beads for effective adsorption of methylene blue dye from aqueous solution, Int. J. Biol. Macromol. 114 (2018) 1315–1324, <https://doi.org/10.1016/j.ijbiomac.2018.04.008>.
- [44] J. Gao, Y. Qin, T. Zhou, D. Cao, P. Xu, D. Hochstetter, Y. Wang, Adsorption of methylene blue onto activated carbon produced from tea (*Camellia sinensis* L.) seed shells: kinetics, equilibrium, and thermodynamics studies, J. Zhejiang Univ. Sci. B 14 (2013) 650–658, <https://doi.org/10.1631/jzus.B12a0225>.
- [45] Y.E. Mouzdahir, A. Elmchaouri, R. Mahboub, A. Gil, S.A. Korili, Equilibrium modeling for the adsorption of methylene blue from aqueous solutions on activated clay minerals, Desalination 250 (2010) 335–338, <https://doi.org/10.1016/j.desal.2009.09.052>.
- [46] S. Azizian, Kinetic models of sorption: a theoretical analysis, J. Colloid Interface Sci. 276 (2004) 47–52, <https://doi.org/10.1016/j.jcis.2004.03.048>.
- [47] F.-C. Wu, R.-L. Tseng, R.-S. Juang, Characteristics of Elovich equation used for the analysis of adsorption kinetics in dye-chitosan systems, Chem. Eng. J. 150 (2009) 366–373, <https://doi.org/10.1016/j.cej.2009.01.014>.
- [48] J. López-Luna, L.E. Ramírez-Montes, S. Martínez-Vargas, A.I. Martínez, O.F. Mijangos-Ricardez, M.D.C.A. González-Chávez, R. Carrillo-González, F.A. Solís-Domínguez, M.D.C. Cuevas-Díaz, V. Vázquez-Hipólito, Linear and nonlinear kinetic and isotherm adsorption models for arsenic removal by manganese ferrite nanoparticles, SN Appl. Sci. 1 (2019) 950, <https://doi.org/10.1007/s42452-019-0977-3>.
- [49] S. Sharma, A. Hasan, N. Kumar, L.M. Pandey, Removal of methylene blue dye from aqueous solution using immobilized *Agrobacterium fabrum* biomass along with iron oxide nanoparticles as biosorbent, Environ. Sci. Pollut. Res. 25 (2018) 21605–21615, <https://doi.org/10.1007/s11356-018-2280-z>.
- [50] S. Banerjee, M.C. Chattopadhyaya, Adsorption characteristics for the removal of a toxic dye, tartrazine from aqueous solutions by a low cost agricultural by-product, Arab. J. Chem. 10 (2017) S1629–S1638, <https://doi.org/10.1016/j.arabjc.2013.06.005>.
- [51] B. An, Cu(II) and As(V) adsorption kinetic characteristic of the multifunctional amino groups in chitosan, Processes 8 (2020) 1194, <https://doi.org/10.3390/pr8091194>.
- [52] F.-C. Wu, R.-L. Tseng, R.-S. Juang, Initial behavior of intraparticle diffusion model used in the description of adsorption kinetics, Chem. Eng. J. 153 (2009) 1–8, <https://doi.org/10.1016/j.cej.2009.04.042>.
- [53] S. Tiwari, A. Hasan, L.M. Pandey, A novel bio-sorbent comprising encapsulated *Agrobacterium fabrum* (SLA731) and iron oxide nanoparticles for removal of crude oil co-contaminant, lead Pb(II), J. Environ. Chem. Eng. 5 (2017) 442–452, <https://doi.org/10.1016/j.jece.2016.12.017>.
- [54] R.R. Krug, W.G. Hunter, R.A. Grieger, Enthalpy-entropy compensation. 1. Some fundamental statistical problems associated with the analysis of van't Hoff and Arrhenius data, J. Phys. Chem. 80 (1976) 2335–2341, <https://doi.org/10.1021/j100562a006>.